## T.2: Generation of Energetic Ultrashort Laser Pulses, Spatio-temporal Shaping and Applications

*Avnish Sharma (aksharma@rrcat.gov.in)*

Since the invention of the chirped-pulse amplification (CPA) technique, terawatt to petawatt class CPA laser systems [1] have been built and laser systems capable of delivering laser peak power much beyond petawatt level are under construction in several laboratories around the world. In particular, the Ti:sapphire based CPA laser systems have become standard table-top source of powerful femtosecond laser pulses because of their capability to support broadband amplification, high energy storage, and large thermal conductivity. The energetic laser pulses are being employed in various scientific and industrial applications, and to explore new horizons in almost every scientific field such as material processing, production of ultrafast source of particles and radiation, high-order harmonic generation, and particle acceleration. Next, shaping of the spatial (or transverse) and the temporal (or longitudinal) profiles of ultrashort pulse laser beams is highly desirable for a number of scientific research and industrial applications either to increase the yield or to tailor the outcome of an experiment. For instance, generation of low-emittance photo-electron beam for accelerators, optical parametric amplifiers, laser micro-machining etc. requires a flat-top laser pulse.

In this article, we report 1) design and development of a terawatt class Ti:sapphire laser system, 2) use of the energetic laser pulses in nonlinear optical experiments, surface modification of metal and semiconductor mirrors, and 3) spatio-temporal shaping of laser pulses and its beam transport, in three sections. The present work [2-6] has been carried out at Brookhaven National Laboratory (USA) during last two years.

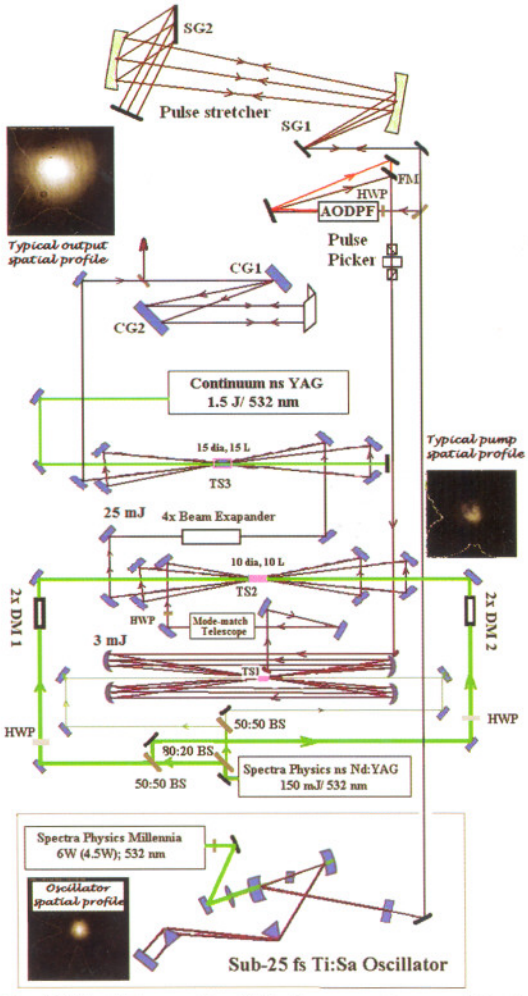


*Fig. T.2.1: Schematic of the laser system and typical spatial profiles at different stages*

### 1. Design and development of a terawatt class Ti:Sapphire Laser system

The laser system [2] was designed to have a sub-25 fs home-built Ti:sapphire oscillator, an all-reflective double-pass pulse stretcher, a commercial acousto-optic programmable dispersive filter (AOPDF) and pulse picker, a highly efficient symmetric confocal 12-pass pre-amplifier followed by two 4-pass power amplifiers and beam optics, and finally a double-pass pulse compressor. The schematic diagram of the laser system is shown in the Fig.T.2.1. The high gain pre-amplifier and first 4-pass amplifier were pumped by a frequency doubled Q-switched Nd:YAG laser (Spectra Physics) delivering nanosecond duration laser pulses with pulse energy of ~125 mJ. The main power amplifier was pumped by another frequency doubled Q-switched Nd:YAG laser (Continuum) delivering nanosecond duration laser pulses having pulse energy of 1.5 J. Both the pump lasers and other sub-units of laser systems (such as AOPDF and pulse picker) were synchronized with laser pulse train from oscillator and were operated at a repetition rate of 10 Hz using a simple and inexpensive synchronization scheme based on only a digital delay generator. The brief description of various sub-systems is given below.

#### 1.1 Femtosecond Ti:Sapphire Oscillator

The oscillator was designed to have a 5 mm optically thick Ti:sapphire crystal (Red Optronics), two curved mirrors of 5 cm focal length (one TNM2 series negative chirp mirror, and another SWP series dichroic mirror from CVI), a 12% output coupler (Newport), along with a high reflecting end-mirror (LGVD series mirror from CVI), arranged in a standard bow-

tie cavity configuration. We explored several combinations of output couplers, cavity, and high-reflecting mirrors of the oscillator to obtain the maximum spectral bandwidth and maximum output power. A Spectra Physics "Millennia" laser (maximum power of 6 watt) pumped the gain medium using a 10 cm focal length lens (PLCX series lens from CVI). The lengths of the non-dispersive and dispersive arms of the resonator were ~68 cm and ~88 cm respectively. Dispersion compensation was achieved by a pair of fused silica prisms separated by 61.5 cm. The oscillator delivered horizontally polarized laser pulses with a FWHM spectral bandwidth of ~50 nm (supporting ~20 fs laser pulse), at a repetition rate of ~89 MHz. The average output laser power was 400 mW at a pump power of 4.5W. We found stable region of mode-locking by optimizing the separation between the two curved mirrors at a given pump power. Stable mode-locking was initiated by tapping the stage holding one of the prisms.

### 1.2 All reflective pulse stretcher

The oscillator pulses were injected into an all-reflective pulse stretcher, consisting of two anti-parallel gratings with a groove density of 1200 l/mm (Spectrogon), two gold-coated concave mirrors (f = 61cm), and a gold coated plane mirror that facilitates a double-pass arrangement by a vertical tilt of ~3.5mrad. The gratings SG1 and SG2 (Fig.T.2.1) were separated from their respective concave mirrors by a distance of ~22 cm and ~32 cm. The stretching factor and the spectral pass-bandwidth of the stretcher were ~5.6 ps/ nm and ~95 nm, respectively, at an incident angle of 450. The throughput of the stretcher was ~25%, limited by the low diffraction-efficiency of the gratings which were used at an incidence angle that was different from the Littrow angle, due to geometrical constraints. The pulse duration after the stretcher was ~150 ps, measured using a 40GHz detector (New Focus 1001) and an analog oscilloscope (Tektronix 7104) with modules 7S11 and 7T11 as sampling and time bases respectively.

### 1.3 Dazzler and single pulse selector

A commercial AOPDF, commonly known as DAZZLER (Fastlite, France), was incorporated after the pulse stretcher, in order to have an active control on laser pulse spectral shape, and to adjust its spectral phase to pre-compensate for the narrowing of the spectral gain, spectral shifting, and changes in the spectral phase during amplification and propagation. The stretched laser pulses from the pulse stretcher were passed through a half-wave plate to preserve the horizontal polarization needed for the downstream optics and the AOPDF, which was externally triggered at 10 Hz in synchronism with the laser pulse train. The diffracted pulses then propagated through a pulse picker (KM Laboratory) to lower the pulse repetition rate to 10 Hz. A flip mount, marked FM in Fig.T.2.1 allows bypassing the AOPDF, if needed.

### 1.4 High gain pre-amplifier and power amplifiers

To achieve the desired overall gain of ~$10^9$ to amplify the laser pulses from sub-nJ to sub-J energy level, the stretched laser pulses were amplified in a high gain 12-pass pre-amplifier and two 4-pass power amplifiers. Instead of using a conventional regenerative amplifier, a multiple pass amplifier (MPA) that reduces the accumulated material dispersion and minimizes the effect of spectral-gain narrowing was used. The preamplifier consists of a Ti:sapphire crystal (10 mm dia., 10 mm long; Red Optronics) placed slightly asymmetrically (45 cm from the pulse injecting concave mirror) inside the confocal configuration formed by four concave mirrors (f=0.5m). A 12 mm diameter mirror was used to extract the amplified pulse. In order to match the pump spatial profile with that of seed, a 1 meter focal length lens, positioned at ~85 cm away from Ti:sapphire crystal, was used to focus the pump beam in a double end pump configuration. The absorption of the pump laser pulse was ~90%. The output pulse energy after 12 passes was ~3 mJ at pump energy of ~25 mJ, giving an overall gain and extraction efficiency of $5x10^6$ and ~12%, respectively, at pump energy fluence of ~2.5 J/cm$^2$ on each arm. This extraction efficiency is much larger than 0.1-3% reported [7] for a symmetric-and an asymmetric- confocal amplifier. Our results are also comparable to those from a well-optimized double confocal amplifier (~19%) [8]. Improved extraction efficiency has been attributed to the better spatial and temporal overlap between the pump and seed beams. This can be improved further by using a tighter focusing geometry, but at the cost of increased misalignment sensitivity.

The pre-amplified pulse is then sent to a beam-expanding telescope (f=125 mm, & f=-75 mm), and then to the 4-pass power amplifier (MPA2), consisting of a Ti:sapphire crystal (10 mm dia., 10 mm long; Red-Optronics). This amplifier was pumped by additional two beams, each having pulse energy of ~50 mJ, derived from the same frequency-doubled Q-switched Nd:YAG laser. Two independent 0.5X beam expanders, DM1 (f=100 mm & f= -50 mm) and DM2 (f=150 mm & f= -75 mm), gave a pump-beam diameter of ~3 mm on the amplifier crystal, to attain a pump fluence of ~1.5 J/cm$^2$. The amplified spectrum after MPA2 had a spectral bandwidth of 30 nm and 20 nm (FWHM), with and without AOPDF, respectively.

The amplified energy after first power amplifier was measured to be ~25 mJ per pulse with ±15% fluctuations (peak-to-peak) in 4 hours of continuous operation. Without any ASE suppression controls, it has an estimated ASE background ratio of 1:20, assessed from the measured pulse energy with and without seeding the amplifiers. The last 4-pass power amplifier MPA3 consisted of a Ti:sapphire crystal (15 mm dia., 15 mm long; Crystal Systems) and is pumped by

continuum laser. To minimize the variation in the pulse energy and ASE due to beam misalignment caused by variation in temperature and humidity conditions in the laboratory, low-cost video cameras were installed to monitor the input and amplified output beams at different locations and to correct their spatial position.

## 1.5 A Novel and simple synchronization scheme

For efficient pulse amplification, stretched pulse must reach the amplifiers in synchronism with the pump laser pulse at an optimum time. Next, other sub-systems such as Dazzler and pulse picker also require low-repetition rate synchronized trigger signals with respect to the laser pulse train from the oscillator. Conventionally, both the objectives are achieved by generating low repetition rate synchronized trigger signals using a frequency divider and a digital delay generator to provide appropriate temporal delays. In the present work, we demonstrated a simple, low-cost alternative synchronization scheme [2] using only a digital delay-generator (Stanford DG535). The latter was triggered directly by the amplified 89 MHz signal derived from laser oscillator using a fast silicon detector (rise time < 300 ps) and Stanford 300 MHz amplifier (SR440). The low-frequency trigger signals were generated by setting the delay to one of its output channel (D) slightly smaller than the time period (1/ftr) of the desired trigger rate (ftr). Thus, for 10 Hz signals, this delay was set at 99.9 ms. The minimum and maximum trigger rate as dictated by the longest allowed delay and minimum cycling time of the delay generator, were 1 mHz, and 1 MHz, respectively. Once the digital delay-generator was triggered by one of pulses of the train, rest of trigger pulses are ignored till the D delay is over and then re-triggering takes place, thus effectively generating low frequency synchronized trigger signals. The delay outputs namely To, A, B, and C from the delay-generator were then used to trigger the AOPDF, firing the flash lamps, Q-switch, and activating the pulse picker respectively.

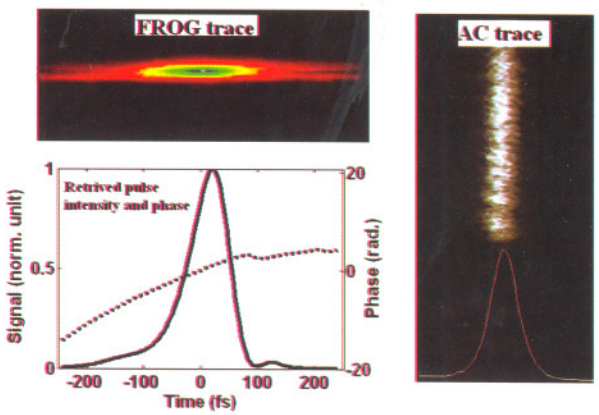


*Fig.T.2.2: Measured FROG and AC trace, and retrieved pulse using FROG. Horizontal-vertical axes are, respectively, the time-wavelength in FROG trace, and the time-space in the AC trace.*

### 1.6 Pulse compressor

Prior to the pulse compression in the grating pair pulse compressor, the beam diameter of the amplified pulse was increased 4 times using a beam expander (f=-100 mm, & f=400 mm). The compressor consisted of two 1200 lines/mm diffraction gratings, kept parallel to each other, and a retro-reflecting mirror for making a double-pass arrangement. The incidence angle on the compressor gratings has to be close to that of stretcher for perfect dispersion compensation. However, to increase the energy throughput of the compressor up to 70%, we chose an angle of incidence of $35^0$ (instead of $45^0$) with a grating separation of ~62 cm. We achieved pulse compression down to 80 fs, as shown in Fig.T.2.2. Thus, using pre-amplifier and first power amplifier only, we have generated laser pulses with power level exceeding 0.2TW. With last amplifier, it is expected to reach a power level in range 5-10TW. The characterization of last amplifier is in progress. The compressed pulses were characterized via conventional intensity autocorrelation and SHG FROG. Bypassing the AOPDF yielded a compressed pulse of ~100 fs. The estimated pulse-width for measured bandwidth of 30 nm was ~25 fs. This difference is attributed to the deliberate mismatch between the stretcher and the compressor.

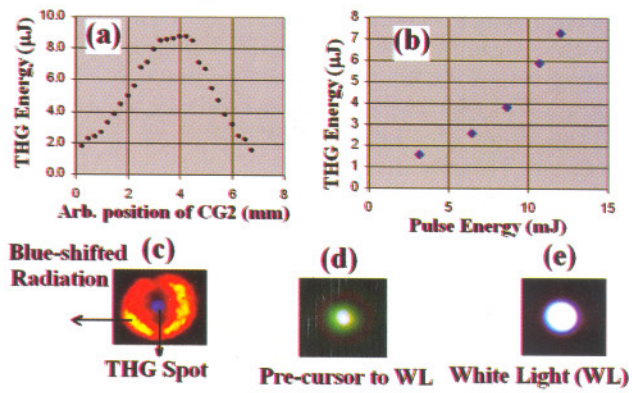


*Fig.T.2.3: (a) THG w.r.t. grating separation; (b) Energy scaling of THG ; (c) Spatial image of THG; (d) Precursor to white-light generation (WLG); and, (e) WHG in fused silica.*

## 2. Applications of the laser system

To demonstrate the applicability of the laser system, two set of experiments were conducted [2]. First, efficient third-harmonic radiation was generated in air using tight focusing conditions and then white light was generated in the fused silica. To obtain the third harmonic generation (THG) signal, and white light, the amplified compressed beam was focused

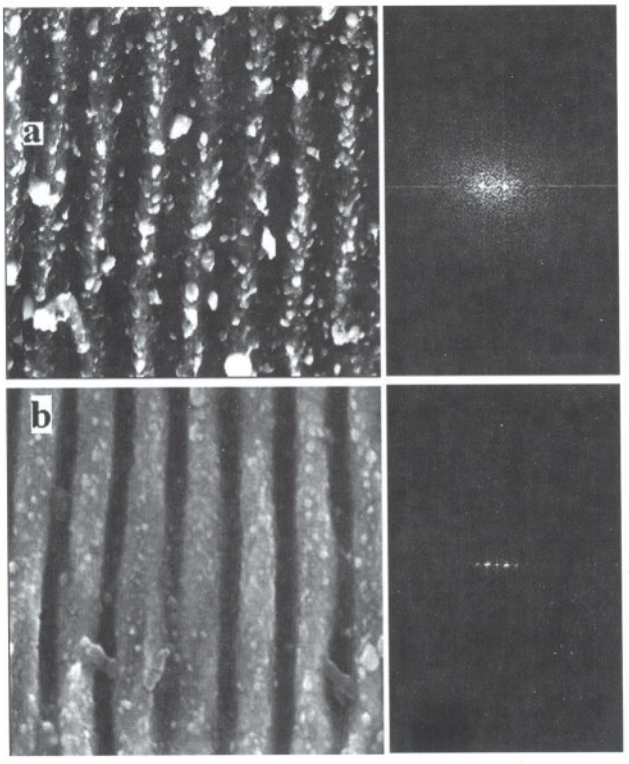


*Fig.T.2.4: SEM images (left) and corresponding 2-D Fourier transform (right) demonstrating imprinting of sub-wavelength surface gratings with (a) and without nano-particles (b).*

in ambient conditions using a 10 cm focal length lens, and then re-collimating the beam using another quartz lens of 12.5-cm focal length. The third harmonic radiation, filtered spectrally with a quartz prism, was monitored by a pyro-electric joule meter. We explored the effect of pulse chirp on THG (Fig.T.2.3a) by changing the separation between the compressor gratings. Having maximized the THG signal at the optimum grating separation, its power scaling with the input pulse energy was obtained (Fig.T.2.3b). The spatial profile of the THG signal recorded using a digital camera also is shown in Fig.T.2.3c. The overall efficiency of the THG was 0.07%, in accordance with that reported in the literature [9]. Interesting, the THG was also accompanied by a blue-shifted radiation (>300nm) that occurred in a preferential cone of ~6$^{0}$ from the laser propagation. After placing a piece of 15 mm thick fused silica (FS) before the focus of the first lens, white-light was produced, as depicted, respectively, in Figs.T.2.3d and T.2.1.3e for the FS plate located at ~5 cm and ~8 cm from the first lens.

In the second set of experiments, only the pre-amplifier output was used to study the formation of sub-wavelength gratings on metal (eg. Cu, Mo etc) mirrors, and on Si surface, for variety of applications. Grating formation over large sample area was achieved by raster scanning the sample at a fixed beam. Fig.T.2.4 illustrates the typical SEM images and corresponding 2-D Fourier Transform of sub-wavelength surface gratings generated on a molybdenum mirror recorded using 100 fs duration pulses under two raster scan rate and fluence conditions. The periodicity in range 500-750 nm is observed under different pulse energy fluence. Interestingly, periodicity in range 240-360 nm was also observed (not shown in figure) and is probably due to second harmonic generation at the interface. The periodic structure was always perpendicular to the linear polarization (or major axis of elliptic polarization) of the laser beam. Several parametric studies such as effect of pulse fluence, raster scan rate, incident laser polarization etc. have been performed, the details of which will be presented elsewhere [3].

## 3. Passive spatio-temporal beam shaper

To achieve spatio-temporal shaping of the laser beams, we demonstrated a simple and robust method based on simultaneous use of passive pulse stacker and passive aspheric refractive optical shaper [4]. Pulse stacking was carried out using a set of birefringent crystals and using optical delay lines based on discrete optical elements. It is found that birefringent crystal based pulse stacker is very robust and reliable compared to a delay line based stacker. An optical beam transport system has been designed and built to deliver the spatio-temporal shaped ['beer-can' shape] laser beam onto a photo-injector [5] located at ~9 m from the beam shaper. Experimental studies on spatio-temporal shaping have been validated theoretically. While pulse shaping was simulated using MATLAB, the optical design software ZEMAX was used to simulate the beam shaper, its alignment tolerance, and to study the beam transport. Theoretical and experimental details are given in ref.4, while brief summary of the experimental results is given below.

### 3.1 Description of the pulse shaper

It uses three birefringent (a-cut YVO4) crystals of thickness of 24 mm, 12 mm and 6 mm. Each crystal was oriented in such a way that it generates two replica pulses, whose amplitudes and relative temporal delay are governed by the orientation of crystal relative to incident laser polarization, crystal birefringence and thickness respectively. The pulse shaper has been tested using 10 ps duration s-polarized laser pulses at 532 nm wavelength with an average power of 2.5 W at a repetition rate of 81.25 MHz from a cw mode-locked laser oscillator. In one arm of the home made cross-correlator (Fig.T.2.5), three YVO4 crystals in decreasing crystal thickness were positioned. These crystals were mounted on rotational stages (0.5$^{\circ}$ accuracy) with independent horizontal and vertical tilt adjustments to obtain variable amplitudes and static phase of

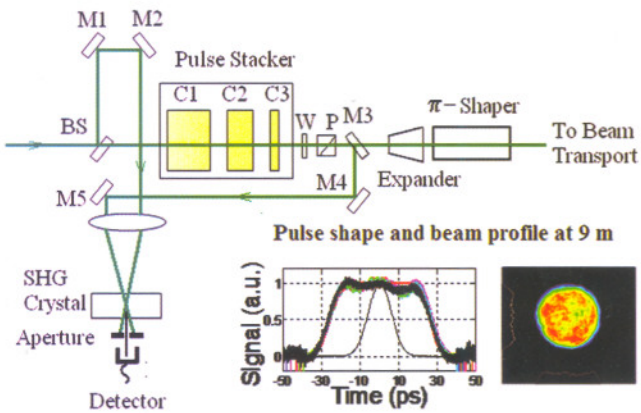


*Fig.T.2.5: Schematic of spatio-temporal shaper. Figure also depict output pulse shapes recorded over 4 hrs, typical de-convoluted (thick black) and theoretical pulse shape (red line) and incident laser pulse ( thin black line) and beam profile at 9m.*

the various replica pulses. The temporal delay among the replica pulses was calculated to be 1.1 ps / mm from the measured crystal birefringence of 0.33. A half-wave plate and a polarizer were placed after the stack to rotate the polarization of the output beam to match with that of the reference pulse on the other arm. The half- wave plate, polarizer, beam splitter, and the mirror M3 were mounted on flip mounts so that the shaped beam can be directed either to the cross-correlation measurement or to the beam shaper, beam transport system and finally to photocathode target. The overall transmission of the three YVO4 crystals was ~62%, which gave an intrinsic absorption loss of ~ 0.116 $cm^{-1}$. Due to the non-zero optical absorption, the thermal expansion of the crystals, and the temperature dependence of their birefringence, lead to a time dependent variation in the differential phase shifts among replica pulses. Hence, the crystals were allowed to reach thermal equilibrium ~1 hour prior to the alignment of the crystals. This stabilization procedure was found to be important to yield a reproducible flat-top pulse routinely. A near flat-top pulse profile with FWHM duration of ~53 ps was obtained. It has a rise and fall time of ~10 ps as dictated by the initial pulse width. The intensity modulation over the flat-top region was calculated to be ~9% (rms). The flat-top temporal profile was recorded at 10 minutes interval over 4 hours of continuous operation, demonstrating its short and long term stability in a standard laboratory environment.

In such a scheme, one may also generate other pulse shapes by changing the amplitudes, temporal delay, phase shifts which can be simply changed by changing the tilt angle of each crystal or by changing crystal temperature, and also by changing pulse chirp of replica pulses. Shaping of shorter duration laser pulses will require thinner crystals leading to better overall transmission. For longer duration pulses, either a crystal with lower loss coefficient or hybrid design using both crystals based stacker and optical element based stacker should be used. Such a hybrid stacker is being tested for its use in the Energy Recovery LINAC being built at BNL. Since the spectral transmission of the YVO4 crystal is limited from 500 nm to 5000 nm, for temporal shaping in the UV spectral regime, birefringent crystals such as -BBO and quartz should be employed.

### 3.2 Spatial beam shaper and beam transport

A spatial flat-top beam was achieved using a refractive beam shaper, known as π-shaper, which consisted of two fused silica plano-convex aspheric lenses, arranged with the convex surfaces facing each other. The π-shaper was optimized at its operation wavelengths of 532 nm and the separation between aspheric lenses was set at 149.8 mm. In order to match the optimum input beam size at the refractive beam shaper, the input laser beam from laser oscillator was magnified by using a 3.5X beam expander, consisting of a plano-concave and a plano-convex lens of focal length - 100 mm and +350 mm, respectively. Simulations of the beam transport suggested that a flat-top laser beam is more prone to diffraction and develop strong diffraction rings at long propagation distance. The depth of focus, the distance over which flat-top profile does not develop diffraction rings, is found to be ~50 cm for this configuration.

The photo-injector of an accelerator is typically located many meters away from the laser room. Therefore, in addition to obtaining a flat-top spatial beam profile, it is essential to develop an optical beam transport system to deliver the flat-top beam profile onto the photo-cathode. A Keplerian image relay magnifier / de-magnifier system was designed. It consisted of two identical plano-convex lenses with focal length of ~2.25 m separated by 4.5± 0.01 m. Fig.T.2.6a depicts the ZEMAX simulated ray diagram of the π-shaper and the schematic of a beam transport system, while Fig.T.2.6b shows the simulated beam profiles of the input beam, the output beam, output beam freely propagated to a distance of 9 m. The output beam image was finally relayed to a distance of 9 m from the πshaper. The corresponding experimental beam profiles are given in Fig.T.2.6c.When the input Gaussian beam profile had a beam waist diameter of 4.7 mm, the π-shaper produced a high quality flat-top beam profile with a diameter of 6.5 mm FWHM. The experimental beam profiles agree well with the ZEMAX simulations. At a distance of 10 cm away from the π-shaper and at 9 m distance with image relay system, the intensity modulations in the measured spatial beam profile was calculated to be ~7% (rms) and ~10% (rms) respectively over the flat region. Despite the number of mirrors and lenses in the image relay system, the flat-top beam

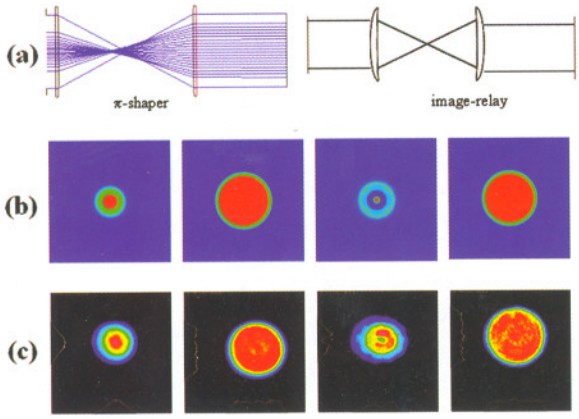


*Fig.T.2.6: Simulated and measured beam profiles: (a) left: ZEMAX simulated ray diagram for the -shaper (vertical scale expanded by 10X), right: schematic of the image relay system; (b) left to right: ZEMAX simulated beam profiles of input beam, output flat-top beam at a distance of 10 cm, at 9 m from the π -shaper without image relay lens, and at 9 m with image relay; (c) Corresponding experimentally recorded beam profiles.*

profile was fairly undistorted. The optical transmission of -shaper was measured to be ~92%.

The angular misalignment (or tilt) and laser beam de-center (or beam lateral offset) relative to the axis of -shaper may result in a distorted output profile. ZEMAX was used to examine the tolerance on the misalignment up to ±9 mrad tilt angle and de-center up to ±0.38 mm. This was then verified experimentally. The experimental results agree well with the simulation.

The tolerances in the beam de-center and tilts were inferred to be within ±20μm and ±0.5mrad, respectively. Similarly, the tolerance on the input beam size was ±60μm at the optimum beam waist diameter of 4.7 mm. These tolerances also dictate the beam pointing error of an input laser beam. Presently, the beam pointing error is ~ 25μ rad per degree change in the environment temperature. In order to obtain different beam size on the photocathode, an image relay beam expander with magnification factor other than unity, an additional beam magnifier / de-magnifier may be placed after the π-shaper. Both the schemes were tested and found to have similar results. While the depth of focus increases with the beam magnification, it decreases with the demagnification of the laser beam. For instance, with a 2X de-magnifier placed after the -shaper, the depth of focus was reduced from ~ 25 cm to ~ 15 cm. The flat-top beam profile was also imaged onto the photo-cathode using a single imaging lens. However, in this arrangement, the output beam cannot be collimated.

### 3.3 Spatial-temporal shaping and transport

The spatio-temporal shaping has been achieved by cascading the temporal pulse shaper and the π-shaper together [6]. As the -shaper has a limited depth of focus that can affect the cross-correlation measurements, first temporal pulse shaping was performed, followed by the beam expansion, spatial beam shaping. Finally image relay was done through the beam transport system, as shown in Fig.T.2.5. Although, the beam expander can be placed either before or after the temporal pulse shaper, it was found that spatio-temporal shaping was best achieved by placing the beam expander immediately after the temporal pulse stacker. The spatio-temporally shaped beam was image relayed to a distance of 9 m i.e. on phto-cathode of ERL. The final beam profile is shown in Fig.T.2.5. This output beam profile resembles the input with little additional spatial distortion.

In conclusion, design, development and characterization of terawatt class Ti:sapphire laser system using novel synchronization scheme and efficient pre-amplifier has been reported. Experiments have been conducted using this laser. A simple and robust method of generating flattop laser pulses and their transport to several meters has been demonstrated for its use in Energy Recovery LINAC that is being built at Brookhaven National Laboratory, USA.

Author acknowledges the technical support of J. Walsh and W. Smith. This work was supported by U.S. Department of Energy under Contract No. DE-AC02-98CH10886.

**References:**

1. http://www.laserfocusworld.com/articles/266389.
2. A. K. Sharma et al, Proc. of National Laser Symposium-09, Mumbai, India, 2010.
3. A. K. Sharma, et al, Manuscript under préparation.
4. A. K. Sharma et al, Phys. Rev. ST Accel. Beams 12, 033501, 2009
5. D. Kayran et al, Proc. of LINAC08, Victoria, Canada, 2008
6. A. K. Sharma et al, Conference on Lasers and Electro Optics 09 (CLEO), Baltimore, USA, 2009
7. P Georges et al, Opt. Lett. 16, 3, 144, 1999; C. Blanc et al, Opt. Lett.18, 2, 140,1993; A. Ruiz-de-la-cruz et al, J. Mod. Opt. 53, 3, 307, 2006.
8. P.F. Curley et al, Opt. Comm. 31, 72, 1996; A. Antonetti et al, Appl. Phys. B 65, 197,1997;Y. W. Lee et al, Appl.Opt. 47, 7, 1015, 2008.
9. M. L. Naudeau et al, Opt. Exp. 14,13, 6194, 2006; R. Ganeev et al, App. Opt. 45, 4,748, 2006.